ARTICLE

Numerical study on the evaporation process of binary droplets in the smoke agent system

Qianshan Xu[1], Yuan Zong[1,*] and Ling Zhao[1]

[1] School of Chemistry Engineering, East China University of Science and Technology, Shanghai, 200237, China

Abstract

The evaporation behavior of a propylene glycol–water smoke agent system was systematically investigated using computational fluid dynamics, with emphasis on the mechanisms governing selective component evaporation. It was observed that elevating the base plate temperature and increasing the initial water content markedly enhance the overall evaporation rate, highlighting the critical role of thermal conditions and composition in controlling vaporization. Analysis of freely evaporating binary droplets revealed that the component with the lower boiling point dominates the evaporation process, resulting in pronounced selectivity in component loss. Additionally, incorporation of a porous medium significantly accelerates the evaporation rate, and further increases in porosity facilitate more efficient vapor release. These findings provide a comprehensive theoretical framework for the controlled modulation of smoke agent evaporation, offering potential strategies for optimizing smoke generation efficiency in practical applications.

Keywords: Evaporation, Smoke Agent System, Propylene glycol

Submitted: 11 March, 2025
Accepted: 16 May, 2025
Published: 17 December, 2025

Vol. 2026, **No.** 1, 2026.
https://doi.org/10.71442/mari2026-0001

***Corresponding author:**
✉ Yuan Zong
cyf20140421@163.com

Citation
Qianshan Xu, Yuan Zong and Ling Zhao (2026). Numerical study on the evaporation process of binary droplets in the smoke agent system. Mari Papel Y Corrugado, 2026(1), 1–15.

1 Introduction

Propylene Glycol (PG) and Glycerine (VG), as smoke agents, can effectively enhance the aerosol release rate [1]. Talih et al. [2] pointed out that smoke is essentially an aerosol, and the main factors influencing the nicotine content in the smoke are inhalation habits, nicotine concentration, and heating voltage. Dai Yujie [3] investigated the effect of glycerine on the volatile components of tobacco smoke and found that within a certain working temperature range, the smoke agent itself almost does not decompose. The significant premise for smoke generation is the evaporation process of the water content inside the tobacco and the smoke agent. Regarding this evaporation process, Dunk G.J. et al. [4] proposed a thermal diffusion model for droplet evaporation. The study showed that the heat-mass change in the droplet evaporation process is closely related to environmental factors. Convection conditions [5], ambient pressure [6], droplet surface temperature [7], base material of the substrate, heating temperature/power [8], and the composition of the smoke agent[9] all significantly impact the droplet evaporation process.

Considering the special addition process of smoke agents present in both the outer and inner layers of tobacco [10], the inhalation process also involves the migration and evaporation of smoke agents within the porous medium. The liquid phase evaporation process within a porous medium has certain unique characteristics. Halder A. et al. [11] investigated the water evaporation mechanism in the water/fatty liquid mixture inside food. The results indicated that

the evaporation rate of the mixed liquid inside food is highest near the heated wall, with water vapor preferentially diffusing from the heated surface to the relatively cooler interior. The diffusion and condensation of water vapor lead to the formation of a significant pressure gradient inside the food, thus promoting moisture evaporation. Zhang et al. [12] coupled the Eulerian model, VOF multiphase flow model, porous medium model, and Lee phase change model to study the evaporation process of the binary azeotropic mixture of tetrafluoroethane/hexafluoropropane within a porous medium. The results showed that increasing heat flux is beneficial to enhancing the overall evaporation rate. Li Hongru et al. [13] studied the evaporation characteristics of porous media with different porosities. The results indicated that materials with higher porosity are more favorable for increasing the suction rate, thereby enhancing the evaporation rate. Therefore, the impact of porous characteristics on the evaporation behavior of smoke agents should also be emphasized.

This paper constructs a numerical model for the evaporation of binary droplets of propylene glycol-water mixtures in the smoke agent system, quantifying their selective evaporation characteristics. The study investigates the impact of substrate temperature, ambient temperature, and smoke agent component ratios on the droplet evaporation process. Additionally, based on the porous characteristics of the cigarette, the evaporation process of the binary droplets within it is explored. The aim of this study is to understand the evaporation behavior of smoke agent droplets and provide technical guidance for the design and optimization of related cigarette products.

2 Mathematical Model

2.1 Physical Model

This study investigates the evaporation process of smoke agent droplets. The droplet is a binary mixture composed of Propylene Glycol (PG) and water, which do not form an azeotrope [14, 15]. During the evaporation process, the droplet is suspended in air and subjected to the combined effects of gravity and surface tension. Heat is supplied from the substrate at the bottom to establish a thermal boundary condition, promoting gradual evaporation into the vapor phase and subsequent diffusion into the surrounding environment. The computational domain of the physical model is illustrated in Figure 1(a), comprising two regions: the droplet (with an initial radius r of 0.12 mm) and the surrounding environment (with a radius R of 1.2 mm). To simplify the calculation, the following assumptions are made:

(1) The environmental domain is significantly larger than the droplet radius, and the ambient temperature within this domain remains constant at T_0;

(2) The modeled droplet is assumed to be a regular hemispherical shape, with uniform distribution of the mixed components inside the droplet, and the Marangoni effect is neglected [16–18].

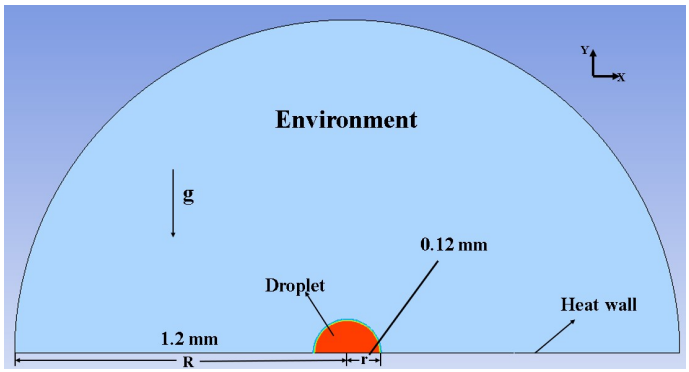

Figure 1. Schematic diagram of the droplet model

2.2 Governing Equations

This study focuses solely on the evaporation process of the droplet, with no condensation occurring at the vapor-liquid interface. Surface tension is assumed to be unaffected by temperature changes and is held constant at 0.072 N/m. The study examines the variation of liquid and vapor components, as well as the average droplet temperature, with time, without considering the deformation of the droplet during the evaporation process [16-18]. Additionally, the effects of the thickness of the heating resistance wire and thermal conductivity are neglected. The governing equations involved in this work include the continuity equation, momentum equation, Mixture multiphase model, species conservation equation, energy equation, and evaporation equation.

(1) Continuity Equation:

The transport equation for the liquid phase volume fraction is given by:

$$\frac{\partial \alpha_l}{\partial t}+\nabla\bullet\left(\alpha_l\bullet\vec{v}_m\right)=-\frac{1}{\rho_m}\sum_{i=1}^{nl}\dot{m}_i -\frac{\alpha_l}{\rho_m}\left(\frac{\partial \rho_m}{\partial t}+\vec{v}_m\nabla\rho_m\right) \quad (1)$$

The transport equation for the vapor phase volume fraction is given by:

$$\frac{\partial \alpha_v}{\partial t}+\nabla\bullet\left(\alpha_v\bullet\vec{v}_m\right)=\frac{1}{\rho_m}\sum_{i=1}^{nv}\dot{m}_i -\frac{\alpha_v}{\rho_m}\left(\frac{\partial \rho_m}{\partial t}+\vec{v}_m\nabla\rho_m\right) \quad (2)$$

The subscript l represents the liquid phase; the subscript v represents the vapor phase; nl and nv represent the number of evaporating components in the liquid and vapor phases, respectively, where nl=nv=2 in this study. The average velocity of the two phases is (Equation 3), m/s; and the average density (Equation 4), kg/m^3; The mass of the evaporating component i is denoted by $\dot{m}_i$, in kg. In the Mixture model, the average velocity is used to calculate the velocities of each phase, and the average density is used to calculate the densities of each phase.

$$\vec{v}_m=\frac{\sum_{k=1}^{n}\alpha_k\rho_k\vec{v}_k}{\rho_m} \quad (3)$$

$$\rho_m=\sum_{k=1}^{n}\alpha_k\rho_k \quad (4)$$

(2) Multiphase Flow Equation:

In this work, the Mixture model is used to solve the two-phase flow, where both phases share the same velocity field:

$$\frac{\partial\left(\rho_m\vec{v}_m\right)}{\partial t}+\nabla\bullet\left(\rho_m\vec{v}_m\vec{v}_m\right)=-\nabla\rho_m+\nabla\bullet\left[\mu_m\bullet\left(\nabla\vec{v}_m+\nabla\vec{v}_m^{\,T}\right)\right] +\rho_m\vec{g}+\vec{F}+\nabla\bullet\left[\sum_{k=1}^{n}\alpha_k\rho_k\vec{v}_{dr,k}\vec{v}_{dr,k}\right] \quad (5)$$

In the equation, $\vec{F}$ is the surface tension of the droplet, in N; μ_m is the mixture dynamic viscosity, in m^2/s, which is calculated using the viscosity formula for a multiphase miscible liquid:

$$\mu_m=\left(\sum_{i=1}^{n}x_{l,i}\mu_{l,i}^{\frac{1}{3}}\right)^3 \quad (6)$$

(3) Turbulent Viscosity Equation:

The $k-\omega$ model is advantageous in handling low Reynolds number flows and turbulence near wall regions [19]. In droplet evaporation simulations, the boundary layer flow near the gas flow and droplet surface is relatively strong. Therefore, the SST k-w turbulence model is used for the calculation:

$$\frac{\partial(\rho k)}{\partial t}+\frac{\partial\left(\rho k u_{l,i}\right)}{\partial x_{l,i}}=\frac{\partial}{\partial x_{l,j}}\left(\Gamma_k\frac{\partial k}{\partial x_{l,j}}\right)+G_k-Y_k+S_k+G_b \quad (7)$$

$$\frac{\partial(\rho\omega)}{\partial t}+\frac{\partial\left(\rho\omega u_{l,i}\right)}{\partial x_{l,i}}=\frac{\partial}{\partial x_{l,j}}\left(\Gamma_\omega\frac{\partial\omega}{\partial x_{l,j}}\right) +G_\omega-Y_\omega+D_\omega+S_\omega+G_{\omega b} \quad (8)$$

For the above equation, the effective diffusion coefficient is calculated as $\Gamma_k=\mu_m+\frac{\mu_t}{\sigma_k}$, $\Gamma_\omega=\mu_m+\frac{\mu_t}{\sigma_\omega}$, where σ is the turbulent Prandtl number.

(4) Species Conservation Equation:

The species conservation equation for the liquid phase is:

$$\frac{\partial\left(\alpha_l\rho_mY_{l,i}\right)}{\partial t}+\nabla\cdot\left(\alpha_l\rho_mY_{l,i}\vec{v}_m\right) =\nabla\cdot\left[\alpha_l\rho_mD_{l,i}\nabla Y_{l,i}-Y_{l,i}\sum_{j=1}^{n}\left(\alpha_lD_{l,i}\nabla Y_{l,i}\right)\right]+\dot{m}_i \quad (9)$$

where $Y_{l,i}$ is the mass fraction of component i in the liquid phase; $D_{l,i}$ is the binary diffusion coefficient of component i in the liquid phase. Since the diffusion coefficients between liquid phase components are generally small, they are neglected.

The species conservation equation for the vapor phase is:

$$\frac{\partial\left(\alpha_v\rho_m Y_{v,i}\right)}{\partial t}+\nabla\cdot\left(\alpha_v\rho_m Y_{v,i}\vec{v}_m\right) =\nabla\cdot\left[\alpha_v\rho_m D_{v,i}\nabla Y_{v,i}-Y_{v,i}\sum_{j=1}^{n}\left(\alpha_v D_{v,i}\nabla Y_{v,i}\right)\right]+\dot{m}_i \tag{10}$$

where $Y_{v,i}$ is the mass fraction of component *i* in the vapor phase; $D_{v,i}$ is the binary diffusion coefficient of component *i* in the vapor phase, which is calculated using the following equation:

$$D_{v,i}=\frac{1-x_{v,i}}{\sum_{j,j\neq 1}^{n}x_{v,i}/D_{v,ij}} \tag{11}$$

In the equation, $x_{v,i}$ is the mole fraction of component *i* in the vapor phase; $D_{v,ij}$ is the diffusion coefficient between components *i* and *j* in the vapor phase, which is further calculated using the Fuller equation:

$$D_{v,ij}=\frac{10^{-2}*T^{1.75}\sqrt{\frac{1}{M_i}+\frac{1}{M_j}}}{p*\left[\left(\sqrt[3]{\sum v_i}\right)+\left(\sqrt[3]{\sum v_j}\right)\right]^2} \tag{12}$$

where *p* is the pressure, in Pa; *T* is the temperature, in K; M is the molar mass, in kg/mol; $\sum v_i$ and $\sum v_j$ are the atomic diffusion volumes of components *i* and *j*, in m^3/kg.

(5) Energy Equation:

$$\begin{aligned}&+\sum_{i=1}^{n}\left[\nabla\left(\alpha_i D_{l,i}\nabla Y_{l,i}\rho_m c_{p,l,i}T\right)\right]\\&+\sum_{i=1}^{n}\left[\nabla\left(\alpha_i D_{l,i}\nabla Y_{l,i}\rho_m c_{p,l,i}T\right)\right]\\&+\alpha_l\rho_m\vec{g}\bullet\vec{v}_m+\dot{q}\nabla\left[\rho_m(c_pT+e_k)\vec{v}_m\right]\\&-\nabla\bullet\left(\lambda\nabla T\right)-\frac{\partial p}{\partial t}=-\frac{\partial\rho_m\left(\sum_{i=1}^{n}\alpha_i\left(c_pT+e_k\right)\right)}{\partial t}\\&-\sum_{i=1}^{n}\left[\dot{m}_i\times\left(L_i+T(c_{p,l,i}-c_{p,v,i})\right)\right]\end{aligned} \tag{13}$$

In the simulation system, the droplet volume is set to be small, and the overall velocity is extremely low, so the viscous dissipation term can be neglected. In the equation, $\dot{q}$ is the given heat flux density, and the heating temperature of the substrate is set to T_{HEAT} in this study. Thus, the heat flux density (Equation 14) is in J/(m^2·s); λ_{wall} wall is the thermal conductivity of the wall, in W/(m·K); $c_{p,l}$ is the liquid phase specific heat capacity at constant pressure, in J/ (kg·K); e_k is the specific kinetic energy, in J/m^2; c_p mix is the specific heat capacity at constant pressure for the mixture phase, in J/ (kg·K); λ is the thermal diffusivity, in J/(m·K·s).

$$\dot{q}=\frac{\lambda_{wall}(T_w-T_i)}{d_i} \tag{14}$$

(6) Evaporation Equation:

$$\frac{\partial\left(\alpha_v\rho_v\right)}{\partial t}+\nabla\cdot\left(\alpha_v\rho_v\overrightarrow{V_v}\right)=\dot{m}_{lv} \tag{15}$$

In the equation, α_v is the volume fraction of the vapor phase; ρ_v is the density of the vapor phase; $\vec{V}_v$ is the dynamic viscosity of the vapor phase; $\dot{m}_{lv}$ is the rate of mass transfer from the liquid phase to the vapor phase, in kg·$(s\cdot m^3)^{-1}$. During the evaporation process, $T_l > T_{sat}$, mass transfer occurs only from the liquid phase to the vapor phase, so:

$$\dot{m}_{lv}=coeff_{eva}*\alpha_l\rho_l\frac{T_l-T_{sat}}{T_{sat}} \tag{16}$$

(7) Evaporation Model in Porous Media:

A single droplet is placed within a porous medium to analyze the characteristics of its heating and evaporation process. Compared to the free evaporation process, the evaporation process within a porous medium is influenced by the resistance of the matrix material to fluid movement, which alters the thermal and mass transfer behavior of the fluid. It is important to note that the structure of real tobacco often exhibits a certain degree of complexity and heterogeneity, which affects the thermal conductivity [20], permeability [21], and stratification phenomena [22] at different points within the porous medium framework. To simplify the model, the porous medium material is assumed to be isotropic [23, 24], and the resistance coefficient *S* in different directions is defined as a source term and introduced into the continuity equations (Equations 1 and 2), as shown below:

$$\frac{\partial \alpha_l}{\partial t}+\nabla\bullet\left(\alpha_l\bullet\vec{v}_m\right)=-\frac{1}{\rho_m}\sum_{i=1}^{n}\dot{m}_i -\frac{\alpha_l}{\rho_m}\left(\frac{\partial \rho_m}{\partial t}+\vec{v}_m\nabla\rho_m\right)+S \tag{17}$$

$$\frac{\partial \alpha_v}{\partial t}+\nabla\bullet\left(\alpha_v\bullet\vec{v}_m\right)=\frac{1}{\rho_m}\sum_{i=1}^{n}\dot{m}_i -\frac{\alpha_v}{\rho_m}\left(\frac{\partial \rho_m}{\partial t}+\vec{v}_m\nabla\rho_m\right)+S \tag{18}$$

$$S=-(R\mu v_i+C\rho|v_i|v_i) \tag{19}$$

In the equation, R is the viscous resistance coefficient, which is the reciprocal of the porosity ε; v_i is the velocity of a certain component i in the liquid phase, where v_i=v_m, in m/s. The definition of porosity is:

$$\varepsilon=\frac{\sum_{i=1}^{nl}V_i+\sum_{j=1}^{nv}V_j}{V} \tag{20}$$

where V is the total volume of the matrix and pores in the porous medium, in m^3; V_i and V_j are the volumes of the liquid and vapor phases, in m^3, and their sum numerically represents the pore volume.

The inertial resistance coefficient C in Equation (19) is represented in the momentum equation as:

$$\frac{\partial(\rho v_i)}{\partial t}+\nabla\cdot(\rho v_i v_i) =-\nabla p+\nabla\cdot\left[\mu_i\left(\nabla v_i+\nabla v_i^T\right)\right]-C\rho|v_i| \tag{21}$$

Considering the migration and diffusion of steam, the total energy equation for each phase in the porous medium is:

$$\left(\rho C_p\right)_{eff}\frac{\partial T}{\partial t}+\left(\varepsilon\alpha_v\rho_v C_{p,v}v_{i,v}+\phi\varepsilon\alpha_l\rho_l C_{p,l}v_{i,l}\right)\cdot\nabla T =\nabla\cdot\left(\lambda_{eff}\nabla T\right)+\dot{q} \tag{22}$$

where $\phi\varepsilon$ is the effective porosity.

2.3 Numerical Simulation Setup

In this work, simulations are performed using the pressure-based solver in Ansys Fluent. The fluid within the computational domain is set to steady-state flow, and the Simple algorithm is used to solve the pressure-velocity coupling terms. The discretization scheme is selected as second-order upwind, with convergence residuals for the continuity equation, velocity, and energy equations set to 10^{-5}. The iteration step size is 0.001 s.

The bottom of the droplet is set as a wall with a no-slip boundary condition, and a constant heating temperature of T_{HEAT} is applied. Under the initial conditions, the temperature of both the droplet and the environment is set to T_0. The farthest outlet from the droplet in the environmental domain is set as a pressure outlet, with the pressure specified as atmospheric pressure. The component properties of the droplet [25] and the physical parameters of the porous medium model [23] are shown in Table 1.

Table 1. Physical property of the droplets and the porous media

		Water		PG	
		liquid	vapor	liquid	vapor
Droplet	Density/ ($kg\cdot m^{-3}$)	1.00×10^{3}	5.54×10^{-1}	1.03×10^{3}	2.01
	Heat capacity/ ($J\cdot kg^{-1}\cdot K^{-1}$)	4182.00	2014.00	2477.10	1837.06
	Thermal conductivity/ ($W\cdot m^{-1}\cdot K^{-1}$)	6.00×10^{-1}	2.61×10^{-2}	2.01×10^{-1}	2.59×10^{-2}
	Viscosity/ $kg\cdot(m\cdot s)^{-1}$	1.00×10^{-3}	1.34×10^{-5}	4.07×10^{-2}	1.16×10^{-5}
	Molecular mass/ ($kg\cdot kmol^{-1}$)	18.02		76.09	
	Molar enthalpy/ ($J\cdot kmol^{-1}$)	-2.86×10^{8}	-2.42×10^{8}	-4.95×10^{8}	-4.08×10^{8}
	Saturation temperature/ K	373.15		460.76	
	Evaporate latent/ ($J\cdot kmol^{-1}$)	4.40×10^{7}		8.72×10^{7}	
	Evaporate frequency	0.1		0.1	
Porous media	Thermal conductivity/ ($W\cdot m^{-1}\cdot K^{-1}$)	2.4×10^{-2}			
	Density/ ($kg\cdot m^{-3}$)	1100			
	Heat capacity/ ($J\cdot kg^{-1}\cdot K^{-1}$)	2080			

This study uses ANSYS ICEM to discretize the computational domain, employing a structured grid division method. Local grid refinement is applied at the wall surface to obtain a high-quality mesh model,

ensuring that the droplet has sufficient grid nodes and improving the computational accuracy.

2.4 Model Validation

To ensure the accuracy of the numerical model, experimental results from the literature [26] are selected for validation. The study in the literature investigated the evaporation process of pure water droplets (with a volume of 5 μL) on a copper heating plate. The experimental environment was at atmospheric pressure with an ambient temperature of 25°C. The experiment used a high-speed CCD camera to capture the morphological changes of the droplet, providing the droplet's profile size variation over time at a heating temperature of 375.15 K. Based on the numerical model presented in Section 1.2 of this paper, simulations were carried out under conditions consistent with the experimental setup in the literature.

Figure 2(a) shows a comparison between the experimental data and simulation results. From the results in the figure, it can be observed that the droplet profile area decreases steadily during the evaporation process, and after 20 seconds, the profile area decreases sharply. This is because, at this point, the droplet surface temperature exceeds the saturation temperature, leading to a significant increase in the evaporation rate, causing the droplet to rapidly dry out. Overall, the trend of the experimental values is in good agreement with the simulation results, with the maximum relative error being 6.63%, indicating that the numerical model is highly accurate. The deviation may be due to the fact that the two-dimensional model used in this study only considers heat transfer in the plane, neglecting energy transfer and dissipation in other directions.

Additionally, a grid independence study was performed on the numerical results. Simulations were conducted using three different mesh sizes: 110,000, 330,000, and 830,000 grid points, with the results shown in Figure 2(b). From the figure, it can be seen that as the mesh size increases, the relative error of the results decreases. When the mesh size was 110,000, the maximum relative error at t=10 s between the simulation and experimental values exceeded 60%. However, when the mesh size reached 330,000, the error between the simulation results and the experimental results was less than 10%. Considering both computational accuracy and resource requirements, it can be concluded that the numerical results are essentially grid-independent when the mesh size reaches 330,000.

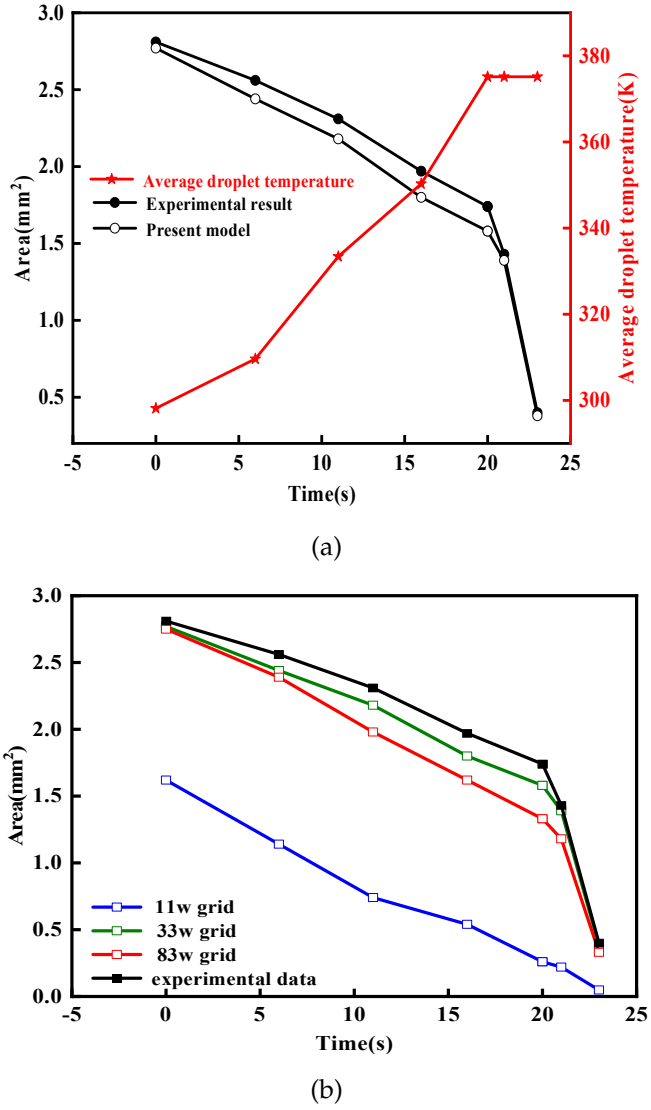

Figure 2. Heat temperature T_{HEAT}=375.15 K: (a) During the evaporate of pure water droplets, the change of profile size with time; (b) Grid independence verification

Furthermore, to further validate the accuracy of the PG-water binary mixture droplet evaporation diffusion model, the numerical results are verified based on the experimental data from Jiang Zhiwu [27], which investigated the volume change of PG-water binary mixture droplets during slow evaporation on a fixed surface. The simulation parameters used in the validation are consistent with the experimental conditions in the referenced literature. As shown in Figure 3, the model validation results are in good agreement. Therefore, it can be concluded that the PG-water binary mixture droplet evaporation calculation results are reasonably accurate.

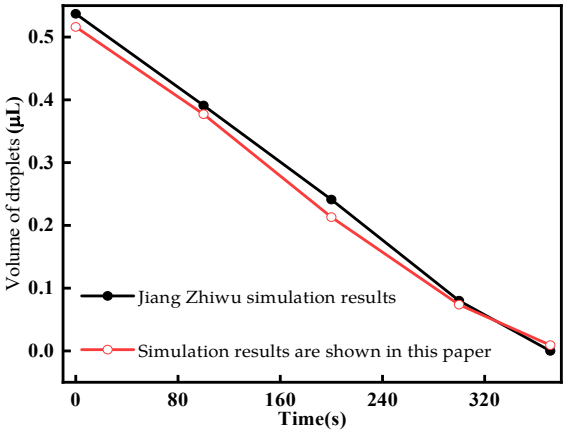

Figure 3. Droplet radius =0.95 mm, droplet center height= 0.364 mm, diffusion coefficient=26.1 mm²/s, $X_{Water,0}$=90%: the relationship between the droplet volume and time during the slow evaporation diffusion process of the droplet

3 Results and Discussion

3.1 Selective Evaporation Process

Under atmospheric pressure, the evaporation temperatures of PG and water are 460.76 K and 373.15 K, respectively. Due to the differences in the evaporation temperatures of the liquid phase components, selective evaporation occurs to varying degrees during the evaporation process of multi-component droplets. Specifically, the lighter component, due to its lower evaporation temperature and smaller latent heat of phase change, evaporates preferentially. This selective evaporation characteristic leads to dynamic changes in the vapor phase composition throughout the evaporation process.

Figure 4 presents the variation of evaporated mass, average droplet temperature, evaporation rate, and vapor phase component content (evaporated mass (water), evaporated mass (PG)) with time during the heating and evaporation of a binary mixture droplet. From Figure 4(a), it can be observed that the average droplet temperature experiences two different trends during the evaporation process. This is closely related to the phase change of the droplet components. Based on the dynamic variations in average droplet temperature and evaporation rate, the entire evaporation process can be divided into three stages:

①Stage 1 (0~0.2 s):As the heating time increases, the overall evaporation rate significantly increases. The average droplet temperature rises from the initial 298.15 K to 480.25 K, which is higher than the evaporation temperatures of both PG and water components. During this stage, both PG and water in the droplet undergo evaporation. The evaporation rates of PG and water are denoted as v_{PG} and v_w, respectively. From the analysis of the evaporation rate ratio v_{PG}/v_w for PG and water components in Figure 4(b), it can be seen that v_{PG}/v_w is relatively small during this stage, indicating that the evaporation rate of water is significantly higher than that of PG, with evaporation predominantly driven by water. Meanwhile, as the temperature continues to rise, the evaporation rate of PG gradually increases. When the temperature reaches 480.25 K, v_{PG}/v_w approaches 0.95.

② Stage 2 (0.2~0.8 s): Between 0.2 and 0.4 s, the evaporation rate of PG gradually approaches that of water, and PG begins to evaporate in large quantities. Due to the relatively high latent heat of phase change for PG, its significant evaporation causes a decrease in the average droplet temperature. However, the total evaporation rate continues to increase and reaches its peak at 0.4 s. Subsequently, between 0.4 and 0.8 s, as the average droplet temperature continuously decreases to 444.31 K, the total evaporation rate correspondingly decreases. At 0.8 s, the evaporation rates of PG and water become nearly equal.

③ Stage 3 (0.8~1.9 s): The average droplet temperature increases again, gradually approaching the temperature of the heating surface. The evaporation rate of PG remains higher than that of water, but the total evaporation rate gradually decreases, ultimately approaching zero, marking the end of the droplet evaporation process. In this stage, PG dominates the evaporation behavior, playing a decisive role in the changes of evaporated mass and component distribution.

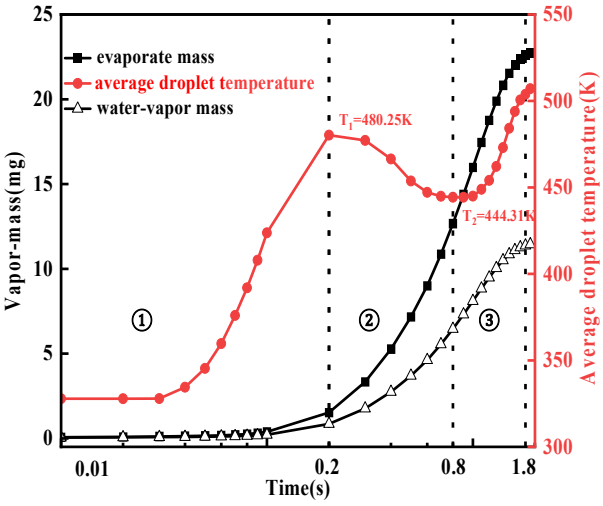

(a)

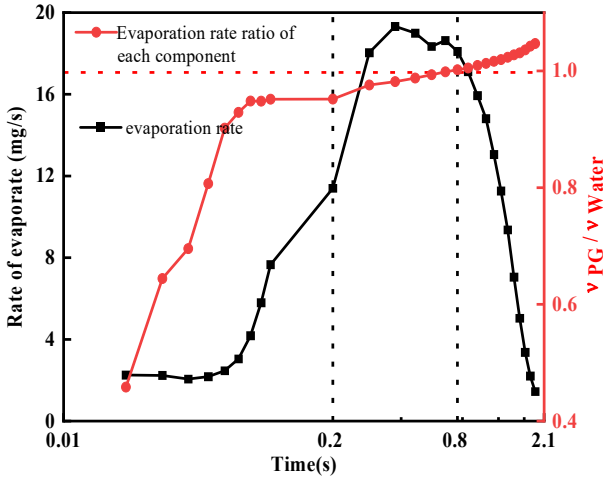

(b)

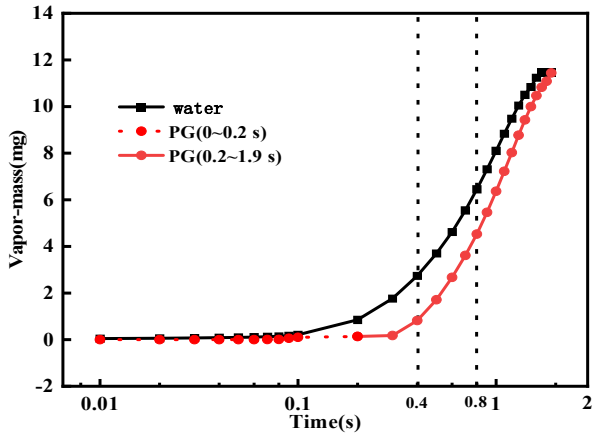

(c)

Figure 4. Droplet evaporate process (the content of water in the droplet $X_{Water,0}$=50%, environment temperature T_0=298.15 K, heating temperature T_{HEAT}=523.15 K): (a) evaporate mass, average droplet temperature; (b) rate of evaporate; (c) vapor mass(water), vapor mass(PG)

The three evaporation stages above reveal the "selective evaporation" phenomenon in binary mixture droplets caused by the differences in the evaporation temperatures of the components. Water, having a lower evaporation temperature than PG, primarily dominates the evaporation process. As heating continues, PG gradually begins to evaporate and later dominates the process until the droplet fully evaporates. The presence of selective evaporation leads to dynamic changes in the vapor phase composition, as shown in Figure 4(c). From time t=0~0.2 s, the droplet temperature is lower than the boiling point of PG. Due to vapor-liquid phase equilibrium, a small amount of PG evaporates into the vapor phase. When the droplet temperature reaches 480.25 K(t=0.2 s), PG begins to boil, and the amount of PG in the vapor phase gradually increases. This process also reveals that the boiling point of PG is affected by the water content and heating conditions. Thus, environmental parameters (such as substrate temperature, ambient temperature, etc.) and the initial water content of the droplet should not be overlooked, as they can significantly influence the evaporation characteristics of the smoke agent, including evaporation rate and vapor phase component selectivity. These factors can notably alter the kinetics and selective characteristics of the evaporation process. The following section will further explore the impact of these parameters on the evaporation characteristics of binary mixture droplets.

3.2 Factors Affecting Droplet Evaporation

3.2.1 Substrate Temperature

To explore the effect of substrate heating temperature on evaporation selectivity, the evaporation process of binary mixture droplets (PG-water) was calculated under four different substrate heating temperatures: 473.15 K, 523.15 K, 573.15 K, and 623.15 K. The initial water content was set at 70% [28], and both the initial droplet and ambient temperatures were 298.15 K. Figure 5 shows the variation in evaporation characteristics under different heating temperatures. From Figure 5, it is observed that with an increase in substrate heating temperature, the total evaporated mass significantly increases.

Further analysis combining Figure 5(c) and Figure 5(d) indicates that this phenomenon is due to the higher heating temperature providing more heat to the droplet, significantly raising the droplet's average temperature, thus accelerating the instantaneous evaporation rate and correspondingly shortening the evaporation time. The results show that higher heating temperatures not only shorten the total evaporation time but also significantly increase the average evaporation rate.

It is worth noting that despite differences in the evaporation rates of each component at different temperatures, the total evaporated mass at the end of the evaporation process remains equal due to the identical initial droplet mass. However, the higher heating temperature has a complex effect on evaporation selectivity. In the third stage of selective evaporation (PG-dominated evaporation stage) shown in Figure 5(d), the higher heating temperature actually reduces the evaporation rate of

PG. Additionally, under high-temperature conditions, the mass fraction of water in the vapor phase decreases more rapidly, meaning that more PG components evaporate earlier within the droplet (as shown in Figure 5(b)), thereby reducing the effectiveness of selective evaporation.

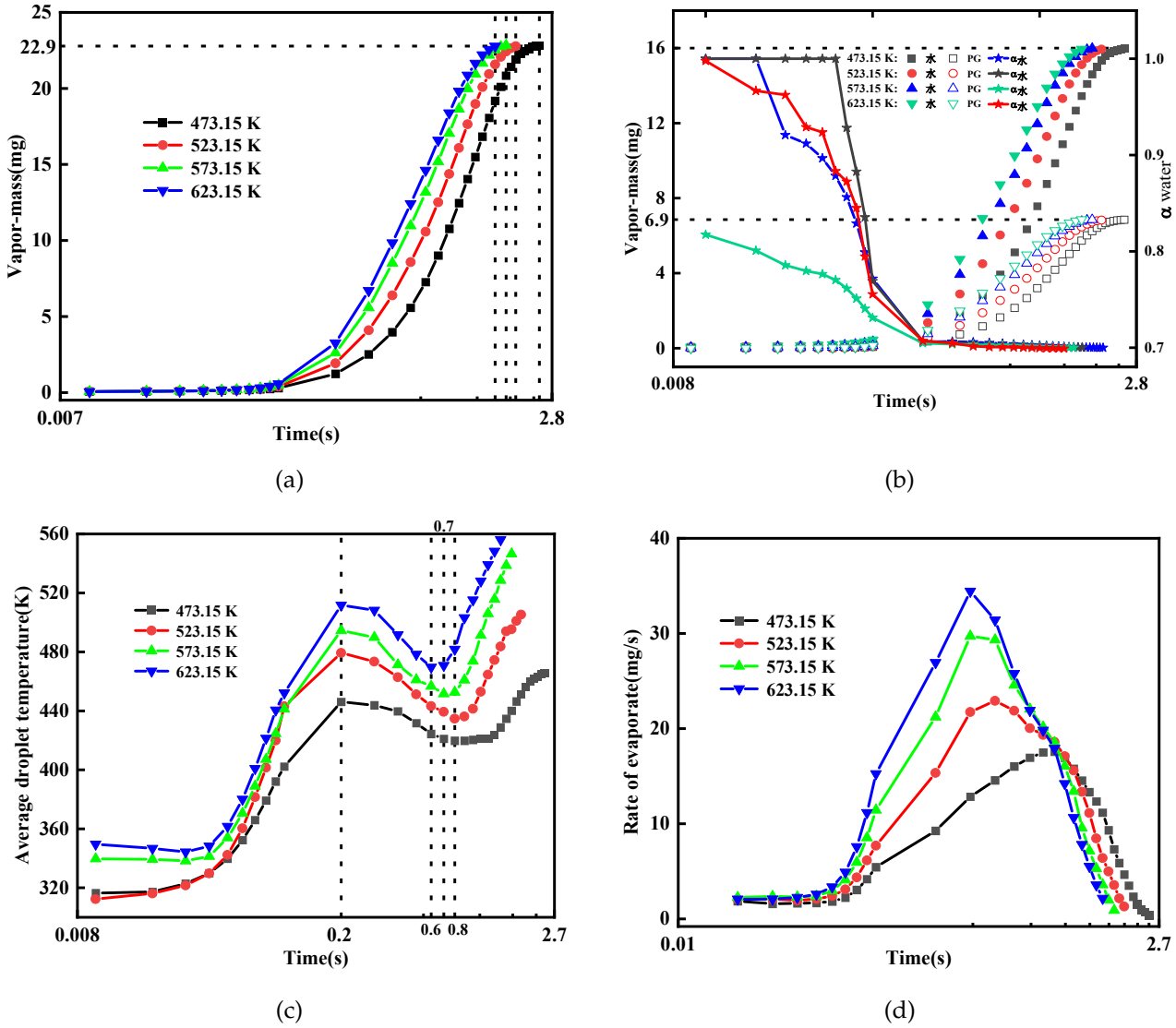

Figure 5. Different heat temperatures ($X_{water,0}$=70%, T_0= 298.15K): (a) evaporate mass; (b) evaporate mass(water), evaporate mass(PG), mass fraction of water in the vapor phase; (c) average droplet temperature; (d) rate of evaporate

This phenomenon is mainly due to the significant impact of temperature on the volatility of liquid phase components in multi-component droplets, with vapor pressure being a major driving force for liquid evaporation. At higher temperatures, the vapor pressure of PG may be higher than that of water, leading to the earlier evaporation of PG. However, as evaporation progresses, the concentration of PG decreases, causing its evaporation rate to drop in the third stage. Furthermore, the evaporation rates of PG and water are influenced not only by temperature but also by the activity coefficients of the liquid phase and the non-ideal behavior of the solution. At higher temperatures, the evaporation rates of PG and water no longer exhibit a simple proportional relationship but are affected by the non-ideal solution behavior, resulting in an earlier decline in the evaporation rate of PG.

The above results indicate that the heating temperature has a significant impact on the evaporation behavior and selectivity of binary mixture droplets. Therefore, during the inhalation process, it is crucial to select an appropriate heating temperature to ensure that the smoke agent can evaporate fully and rapidly into the vapor phase.

3.2.2 Droplet Composition

The moisture in the inhalation process mainly comes from the adsorbed water in the tobacco matrix, as

well as the volatile water in the tobacco itself, with the water content ranging from 53% to 90% [29, 30]. Since the latent heat of phase change of water is lower than that of PG, as the water content in the droplet increases, the overall latent heat of phase change of the mixed droplet decreases. Under the same heat supply, the higher the water content, the faster the evaporation process. Figure 6 shows the trend of evaporation characteristics under different initial water contents (50% to 90%).

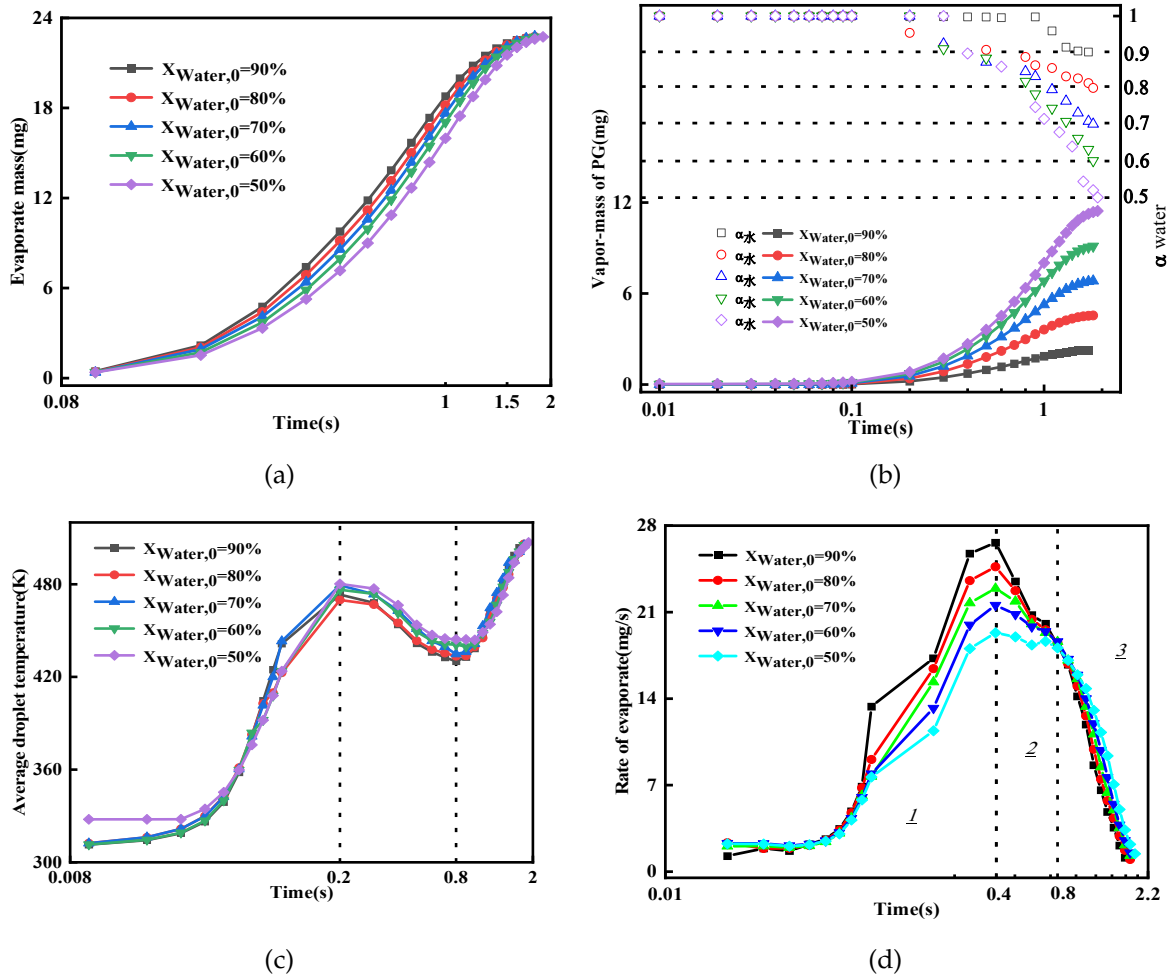

Figure 6. Different initial content of water(T_0= 298.15K, T_{HEAT}= 523.15K): (a) evaporate mass; (b) evaporate mass (PG), mass fraction of water in the vapor phase; (c) average droplet temperature; (d) rate of evaporate

By comparing Figures 6(a) and 6(b), it can be seen that as the initial water content increases, the evaporated mass also increases. However, by comparing the mass fraction of water in the vapor phase, it is evident that during the selective evaporation stage, the amount of PG evaporated decreases. As shown in Figure 6(c), when t = 0.8 s, the average droplet temperature decreases by 36 to 43 K. However, in the third evaporation stage, the influence of water content on droplet temperature is minimal, and the evaporation process is dominated by PG boiling. Since the initial droplet radius is the same for all cases, the total mass of the droplets remains nearly constant. The total evaporation time for droplets with different initial water contents differs only slightly. Further comparison of the evaporation rates shows (as shown in Figure 6(d)) that increasing the initial water content significantly enhances the evaporation rate in the later part of the first stage and the second stage, but the influence on the evaporation rate in the third stage is minimal.

In summary, increasing the initial water content alters the latent heat of phase change of the mixed droplet, significantly affecting both the evaporation rate and droplet temperature, especially enhancing the evaporation rate in the second stage. The increase in water content leads to a reduction in the PG content in the vapor phase. Therefore, it is necessary to control the water content in the tobacco leaves.

3.3 Evaporation of Droplets in Porous Media

Based on the two forms in which the smoke agent exists within tobacco leaves, and under the premise

of maintaining the overall volume of the evaporating droplet constant, the evaporation characteristics of binary mixture droplets with an initial water content of $X_{WATER,0}$=70% in a porous medium with a porosity of 0.75 [23] were first studied. The substrate heating temperature was set to 523.15 K. Figure 7 shows the dynamic changes in evaporated mass, average droplet temperature, and evaporation rate for both evaporation modes. Table 2 lists the average evaporation rates for both modes, with T_{max} representing the highest average temperature during the droplet evaporation process.

Table 2. Evaporate of porous media and free evaporate

Evaporation Mode	t_{total} s	v_{ave} mg·s^{-1}	T_{max} K
Porous Media Evaporation	0.9	29.34	489.4
Free Evaporation	1.8	9.74	479.3

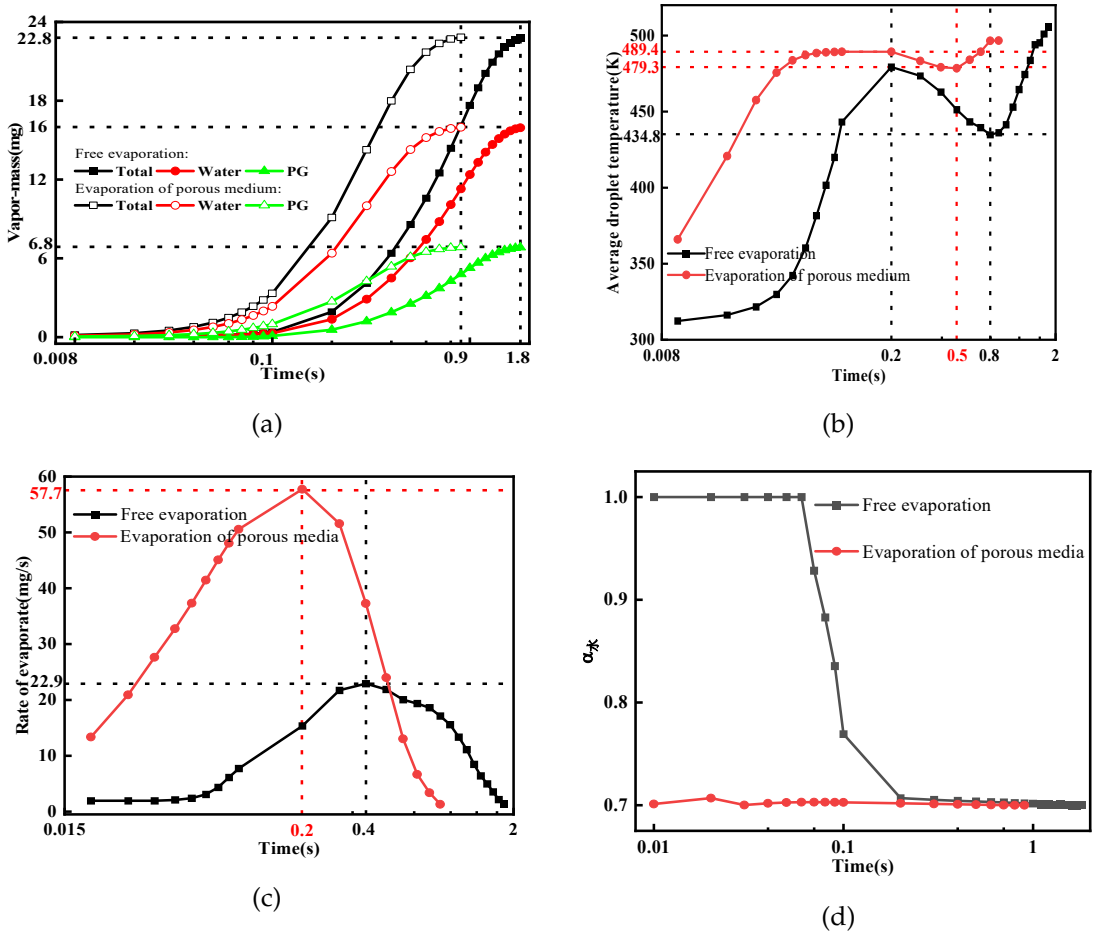

Figure 7. Evaporate of porous media and free evaporate($X_{water,0}$=70%,T_0= 298.15K,T_{HEAT}= 523.15K): (a) evaporate mass(total, water, PG); (b) average droplet temperature; (c) rate of evaporate;(d) mass fraction of water in the vapor phase

It is evident that, compared to free evaporation, when considering the resistance of the porous medium to the liquid phase, both the evaporation rate and the average droplet temperature increase significantly. This phenomenon can be attributed to the porous structure's enhancement of heat and mass transfer during the droplet evaporation process. Comparing Figures 7(a) and 8(c), it can be observed that, in the porous medium evaporation process, the evaporated mass and instantaneous rate are higher at each moment compared to free evaporation.

This phenomenon is related to the liquid film evaporation mechanism [31], where a liquid film forms on the surface or pore walls of the droplet in the porous medium through capillary action. A decrease in the thickness of the liquid film significantly reduces the activation energy required for evaporation [32], thereby enhancing the evaporation rate. It is also associated with the increased heat transfer area; the high specific surface area of the porous medium provides more thermal exchange pathways between the droplet and the medium, facilitating heat conduction and the evaporation process [33]. These mechanisms work together, leading to a significantly higher

evaporation rate in the porous medium compared to free evaporation. Therefore, factors such as porosity, pore size, and surface properties also affect heat transfer efficiency.

At the early stage of evaporation, the droplet temperature gradually increases and then decreases. In the later stage of evaporation, the droplet temperature increases and stabilizes, which corresponds to the temperature changes shown in Figure 7(b). Figure 7(d) shows the change in the mass fraction of water in the vapor phase for both evaporation modes. It can be clearly observed that, compared to free evaporation, the porous medium evaporation mode almost follows the initial mass ratio of water to propylene glycol in the droplet. This indicates that, in the porous medium evaporation mode, the evaporation process of the smoke agent exhibits a non-selective evaporation phenomenon, independent of the boiling point differences. This result is consistent with the findings of Xie Guoyong et al. [34].

Porosity is one of the important parameters that describe the characteristics of porous structures. In actual e-cigarette cartridges, the filling of artificial tobacco typically presents unordered and variable sizes. However, for the sake of simulation, it is assumed that the pore distribution of the porous medium is uniform and isotropic. Figure 8 and Table 3 show the evaporation process of the smoke agent system in the porous medium at different porosities (ε= 0.65, 0.7, 0.75, 0.8, 0.85, and 0.9). Porosity has a significant impact on both the inertial and viscous resistance coefficients of the porous medium. As seen in Equation (19), with the increase in porosity, both the viscous and inertial resistance coefficients decrease, which effectively reduces the flow resistance of the liquid and vapor within the porous medium. This not only increases the heat conduction area between the droplet and the porous medium, enhancing thermal conduction, but also increases the vapor phase due to the higher evaporation rate. This leads to a higher gas flow velocity, further promoting vapor phase convection, which helps to further increase the evaporation rate.

In the first stage of selective evaporation, higher porosity significantly accelerates the instantaneous evaporation rate, and the average droplet temperature also increases. However, after entering the second stage of selective evaporation (t=0.2 s), the total evaporation rate tends to stabilize across different porosity conditions. This phenomenon is determined by the basic principles of the phase change process, mainly depending on the heat capacity of the droplet components. In the third stage, due to the lower evaporation rate of PG components in porous media with lower porosity, the evaporation process completes more quickly.

In conclusion, the variation in porosity significantly affects the heat transfer and flow behavior during the evaporation process in porous media. By appropriately controlling the porosity of the e-cigarette cartridge, the evaporation rate and thermal performance can be optimized, providing valuable reference for the design of related applications.

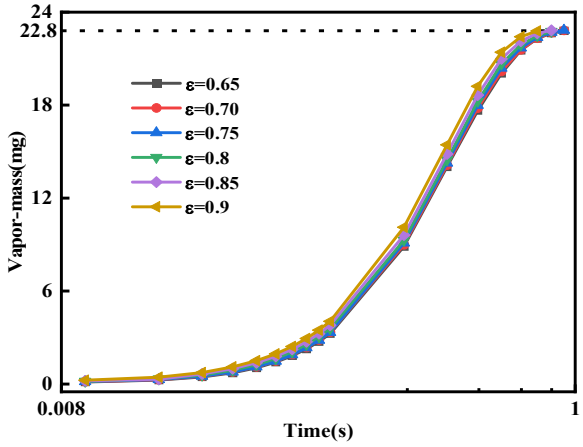

(a)

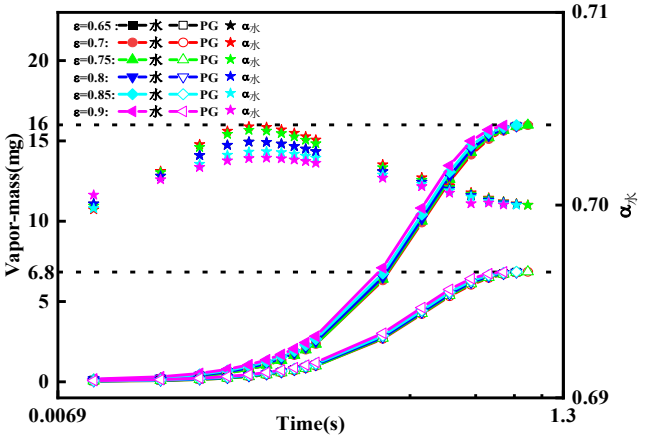

(b)

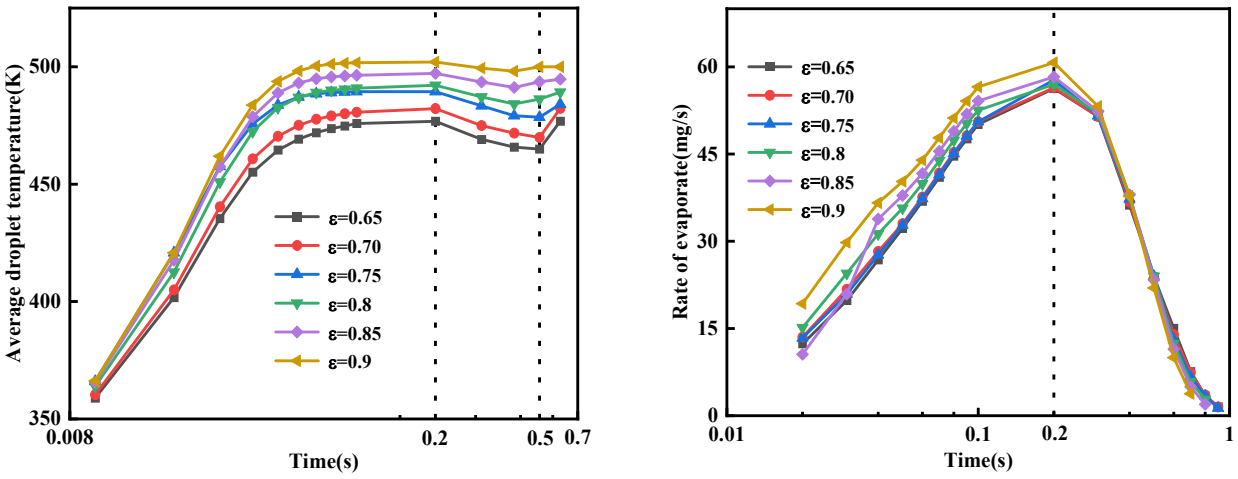

(c) (d)

Figure 8. Different porosities($X_{water,0}$=70%,T_0= 298.15K,T_{HEAT}= 523.15K): (a) evaporate mass; (b) evaporate mass(water), evaporate mass(PG), mass fraction of water in the vapor phase; (c) average droplet temperature; (d) rate of evaporate

Table 3. Rates of evaporate for porous media with different porosities

No	ε	t_{total} s	v_{ave} (mg·s^{-1})
1	0.65	0.9	28.90
2	0.70	0.9	29.39
3	0.75	0.9	30.34
4	0.8	0.8	32.36
5	0.85	0.8	34.49
6	0.9	0.7	37.00

4 Conclusion

This study used CFD simulation methods combined with a porous media model to numerically investigate the evaporation process of propylene glycol-water binary mixture droplets. The main factors influencing evaporation rate and temperature were explored, leading to the following conclusions:

(1) Due to the differences in evaporation temperatures and latent heats of phase change between PG and water, the evaporation process of the binary mixture droplet (PG-water) exhibits selective evaporation characteristics. Water evaporates preferentially, while the heavier component, PG, dominates in the later stages of evaporation.

(2) The evaporation rate and droplet temperature are primarily influenced by the substrate heating temperature and the droplet component ratio, while the ambient temperature has a minimal effect on the evaporation behavior of the binary mixture droplet. Therefore, in the design of related products, it is advisable to increase the substrate temperature and optimize the smoke agent ratio to enhance the smoke volume and improve the user experience. However, the increase in substrate temperature should be strictly controlled within a safe range (not exceeding 350–470°C) [35, 36] to ensure the stability of the smoke agent and the quality of tobacco aroma.

(3) Under the same working conditions, compared to free evaporation, the evaporation rate of the smoke agent in the porous medium, considering resistance effects, significantly increases. Furthermore, the higher the porosity, the higher the evaporation rate. Therefore, to ensure the stability of smoke volume, i.e., the stability of the smoke agent evaporation behavior, the porosity of the e-cigarette cartridge is an important product quality control parameter [37]. Additionally, the ideal porosity range should comprehensively consider evaporation performance, mechanical strength, and structural stability.

References

[1] WANG XIAOFENG, ZHOU SHUN, HE QING, et al. Factors influencing tobacco aerosol release characteristics under heating conditions: Temperature, glycerol, and atmosphere [J]. Tobacco Science and Technology, 2017, 50(10): 48-54.

[2] SOHA T, ZAINAB B, THOMAS E, et al. Effects of user puff topography, device voltage, and liquid nicotine concentration on electronic cigarette nicotine yield: Measurements and model predictions[J]. Nicotine & Tobacco Research, 2014, 1-8.

[3] DAI YUJIE. Experimental study on tobacco pyrolysis behavior and combustion characteristics [D]. Zhejiang: Zhejiang University, 2022.

[4] DUNN G, WILSON S, DUFFY B, et al. A mathematical model for the evaporation of a thin sessile liquid droplet: Comparison between

experiment and theory[J]. Colloids and Surfaces A: Physicochemical and Engineering Aspects, 2008, 323(1-3):50-55.

[5] BIN L, BENNACER R, BOUVET A. Evaporation of methanol droplet on the Teflon surface under different air velocities[J]. Applied Thermal Engineering, 2011, 31(17-18):3792-3798.

[6] DING JIXIAN, SUN FENGXIAN, JIANG RENQIU. Study on the effect of environmental pressure on droplet evaporation under convection conditions [J]. Journal of Harbin Engineering University, 2007, 28(10): 1104-1108.

[7] SHAWN A, ALEJANDRO M, LARRY W, et al. Microdroplet evaporation on superheated surfaces[J]. International Journal of Heat and Mass Transfer, 2012,55(21-22):5793-5807.

[8] SOBAC B, BRUTIN D. Thermal effects of the substrate on water droplet evaporation[J]. Physical Review, 2012,86(2):1.

[9] POURCHEZ J, PARISSE S, SARRY G, et al. Impact of power level and refill liquid composition on the aerosol output and particle size distribution generated by a new-generation e-cigarette device[J]. Aerosol Science and Technology, 2018, 359-369.

[10] HU XIANGHUA, LUO CHONG, WANG RUNAN, et al. Effect of binder type on the formation and physical properties of heat-not-burn tobacco sheets [J]. Chinese Paper Science Journal, 2024, 39(3): 123-131.

[11] HALDER A, DHALL A, DATTA A. Modeling transport in porous media with phase change: applications to food processing[C]. Journal of Heat Transfer-transactions of The ASME,2011,133(3): 031010.

[12] ZHANG B, CUI P, WANG Z, et al. Numerical study on heat and mass transfer of evaporated binary zeotropic mixtures in porous structure[J]. Energies, 2023,16(18):6526.

[13] LI HONGRU, CHEN YAN, ZHANG JINCAO, et al. Evaporation characteristics of porous media with different porosities [J]. Chemical Engineering Journal, 2017, 68(9): 3380-3387.

[14] GAO ZHENGHONG, CUI ZHIYU, LI ZHIWEI, et al. Isothermal vapor-liquid equilibrium of ethanol-butyl acetate binary system [J]. Chemical Industry and Engineering, 1995, (1): 7-10.

[15] WANG SHENG, ZHANG SHUWEI, LI YAN, et al. Separation process of water, propylene glycol, and propylene glycol monomethyl ether mixtures [J]. Petroleum and Petrochemical Engineering, 2002, 31(12): 973-977.

[16] LI JINDA, LIU HUIMENG. Simulation analysis of the evaporation characteristics of n-dodecane droplets [J]. Small Internal Combustion Engine and Vehicle Technology, 2017, 46(3): 38-44.

[17] TAMIN J, HALLETT W. A continuous thermodynamics model for multicomponent droplet vaporization[J]. Chemical Engineering Science,1995, 50(18): 2933-2942.

[18] SAZHIN S, ELWARDANY A, KRUTITSKII P, et al. A simplified model for bi-component droplet heating and evaporation[J]. International Journal of Heat and Mass Transfer, 2010, 53 (21-22):4495-4505.

[19] WILCOX D. Turbulence modeling for CFD[M]. 3rd ed. California, America: DWC Industries, 2006.

[20] DULLIEN F. Porous Media: Fluid transport and pore structure[M]. 2nd ed. California , America: Academic Press,1992.

[21] PRAT M. Recent advances in pore-scale models for drying of porous media[J]. Chemical Engineering Journal, 2002,86(1-2): 153-164.

[22] YIOTIS A, IOANNIS N, ATHANASSIOS K, et al. Coupling between external and internal mass transfer during drying of a porous medium[J]. Water Resources Research,2007,43(6):80.

[23] XIAO WEIQIANG, ZHOU GUOJUN, JIANG JIAN, et al. Numerical simulation of heat transfer and smoke flow in heated cigarette products [J]. Journal of East China University of Science and Technology (Natural Science Edition), 2021, 47(1): 35-40.

[24] DU LIANG. Study on the cigarette smoke flow and diffusion state based on CFD [D]. Guangzhou: South China University of Technology, 2018.

[25] GU SHUO. Transport and surface capillary evaporation mechanisms of propylene glycol-propylene glycol binary mixture in porous media [D]. Tianjin: Tianjin University, 2022.

[26] WANG XIAODONG, LU GUI, PENG XIAOFENG, et al. Experimental study on the dynamic characteristics of evaporating droplets on a heating plate [J]. Journal of Aerospace Power, 2006, 21(6): 1001-1007.

[27] JIANG ZHIWU. The forces between evaporating droplets and their application in droplet manipulation [D]. Anhui: University of Science and Technology of China, 2021.

[28] YANG XUEYAN, WEN GUANGHE, LI FENG, et al. Characterization of heat-not-burn cigarette tobacco materials [J]. Food and Machinery, 2020, 36(5): 205-210.

[29] LI ZHAOJIAN, JIN YONG, ZHOU CHENGXI, et al. Effect of moisture content on the chemical composition of different types of heat-not-burn cigarette tobacco [J]. Food and Machinery, 2019, 35(10): 35-39, 149.

[30] KEN SHENGYE, WEN GUANGHE, YANG XUEYAN, et al. Simultaneous detection of moisture, 1,2-propylene glycol, nicotine, and glycerin in heat-not-burn cigarette tobacco materials by GC-TCD [J]. Tobacco Science and Technology, 2020, 53(5): 41-46.

[31] ZHU XIAOYU. Influence and mechanism of porous media on liquid fuel atomization/evaporation under thermal conditions [D]. Zhejiang: Zhejiang University, 2023.

[32] MEISAM H, SAEED M. Thin liquid films formation and evaporation mechanisms around elongated bubbles in rectangular cross-section

microchannels[J]. International Journal of Heat and Mass Transfer,2020, 163: 120474.

[33] ZHAO Z, AVEDISIAN C. Enhancing forced air convection heat transfer from an array of parallel plate fins using a heat pipe[J]. International Journal of Heat and Mass Transfer,1997,40(13):3135-3147.

[34] XIE GUOYONG, DU WEN, WANG ZHIGUO, et al. "Non-selective evaporation" mechanism and experimental verification of binary system atomizer in porous medium atomizers [J]. Tobacco Science and Technology, 2023, 56(9): 58-69.

[35] CUI HUAPENG, CHEN LI, FAN MEIJUAN, et al. Effect of heating temperature on the physical properties of heated tobacco aerosol [J]. Tobacco Science and Technology, 2022, 55(4): 36-41.

[36] ZHENG XUDONG, LI ZHIQIANG, WANG CHENGYA, et al. Study on the release characteristics of e-cigarette smoke under different heating temperatures [J]. Anhui Agricultural Science, 2018, 46(36): 168-171.

[37] LU LEHUA, GAO JIE, FEI FEI, et al. Release performance of main components of reconstituted tobacco in electric heating cigarettes under different processes [J]. Tobacco Science and Technology, 2023, 56(3): 30-40, 77.